Journal of Alloys and Compounds 509 (2011) L47–L51

Contents lists available at ScienceDirect

Journal of Alloys and Compounds

journal homepage: www.elsevier.com/locate/jallcom

Letter

Preparation and electrochemical catalytic property of Au–Ni alloy with porous structure

Dwight K. Inkrott, Rachael L. Willingham, Tyler Balster, Yong X. Gan*

Department of Mechanical, Industrial and Manufacturing Engineering, College of Engineering, University of Toledo, 2801 W. Bancroft Street, Toledo, OH 43606, USA

ARTICLE INFO

Article history:
Received 12 May 2010
Received in revised form
12 September 2010
Accepted 28 September 2010
Available online 8 October 2010

Keywords:
Porous Au–Ni alloy
Electrochemical dealloying
Carbohydrate oxidation

ABSTRACT

In this work, porous gold–nickel alloy was prepared by electrochemical dealloying in 8.75 wt.% nitric acid. Surface morphology of the dealloyed material was observed by scanning electron microscopy and its composition was revealed by energy dispersive X-ray spectra (EDS). Electrochemical oxidation of carbohydrate on the porous material was studied. It is found that the electrochemical dealloying results in the formation of gold-rich ligaments and nickel-rich pores. The results obtained from electrochemical oxidation of 20% carbohydrate reveal that the porous Au–Ni is more than three times active than the base Au–Ni alloy.

1. Introduction

Understanding electrochemical oxidation of biomass on porous materials is meaningful for sustainable energy research because many agricultural products are degradable and considered as alternative energy sources [1,2]. Preparation and electrocatalytic reactions of porous materials in fluids made from agricultural products have recently been studied [3]. In order to obtain high efficiency catalysts, selective etching has been used to extract certain metallic elements from alloys to form porous structures [4]. Comparative studies on the electrochemical activities of the porous metallic electrodes with bulk metallic catalysts show that the electrocatalytic properties of porous electrodes are enhanced significantly because porous structures have high electroactive surface areas [5]. For example, the electro-oxidation current density of a porous nickel is increased four to six times as compared with that of the bulk nickel electrode for generating power from biomass [6].

Porous materials can be made through different ways. Chemical etching is a well-known and frequently used method for making porous metals [7–9], while co-evaporation may be used for preparation of porous metal oxides [10]. Porous gold has caught special attention because of its chemical stability and surface activity. For example, porous gold has found applications for catalyst support [11], biosensor substrate [12], chemical microactuator [13], filter [14], microreactor [15], and proton exchange membrane fuel cell electrode [16].

Porous Au specimens with ligament-like structures were fabricated by dealloying [7]. Smith et al. [8] prepared porous gold films through dealloying $AuAl_2$. The porous gold has void densities between 45% and 65%. Zhou et al. [9] proposed another way to fabricate porous gold film. The starting materials are copper and gold alloys thin films prepared via vacuum deposition. The formation of ultra-thin porous gold films from the Au–Cu alloy films involved chemical etching by hydrochloric acid or by nitric acid.

It is noticed that preparing porous metals via chemical etching is very difficult to control in view of the reaction kinetics. For example, the change in the concentration of the acids, and the temperature fluctuation in the etchant solutions have significant effects on the ligament morphology, void density and strength of the porous metals. During the process of pore formation, the capillary effect causes surface relaxation and affects the dimension of the porous metals [17]. Another limitation of chemical dealloying is the environmental pollution due to the frequent use of high concentration, volatile enchants such as concentrated nitric acid [18]. High concentration nitric acid is dangerous due to the very strong oxidation behavior and it tends to release poisonous gas, NO_2, during handling. While using diluted nitric acid could eliminate this hazardous gas and reduce the risk. One of the objectives of this work is to develop a better and controllable dealloying process than chemical etching. Preliminary research results of electrochemical dealloying in low concentration acids to generate porous gold–nickel alloys were obtained. The electrocatalytic property of the porous Au–Ni in an agricultural product, table sugar, was also studied.

* Corresponding author. Tel.: +1 419 530 6007; fax: +1 419 530 8206.
E-mail address: yong.gan@utoledo.edu (Y.X. Gan).

0925-8388/$ – see front matter © 2010 Elsevier B.V. All rights reserved.
doi:10.1016/j.jallcom.2010.09.183

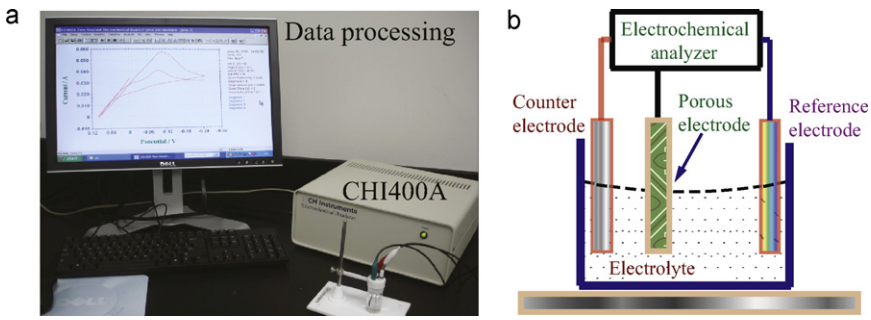

Fig. 1. Experimental setup for dealloying and electrocatalytic property characterization: (a) equipment for experiments and (b) schematic of the electrochemical cell.

2. Materials and experimental methods

Gold–nickel wire with the composition of Au:Ni=82:18 wt.% was purchased from Alfa Aesar. The diameter of the Au–Ni wire was 0.5 mm. Platinum electrode purchased from CHInstrument, Inc. was used as the counter electrode for electrochemical dealloying and electrocatalytic characterization. Chemicals such as nitric acid, sulfuric acid, acetone with ACS purities were used. A biodegradable material, table sugar, was used in characterizing the electrocatalytic behavior of the porous Au–Ni. This product was purchased directly from supermarket. A three-electrode system was set up for both electrochemical dealloying and electrochemical catalytic property characterization. As shown in Fig. 1(a), three electrodes are connected with a CHI400A Electrochemical Quartz Crystal Microbalance. The three electrodes are the Ag/AgCl reference electrode, the work electrode, and the platinum counter electrode as schematically shown in Fig. 1(b).

Electrochemical dealloying was performed for removing alloy elements from the Au–Ni metallic alloy in diluted HNO_3 with the concentration of 8.75 wt.%. The Au–Ni alloy was made into a work electrode. The work electrode was assembled with the Ag/AgCl reference electrode, and the platinum counter electrode in the cell as shown in Fig. 1(b). Under controlled potentials generated by positive cyclic voltammetrical (CV) scan, selective dissolution of metal elements was achieved. As a result, porous Au–Ni was obtained. During the CV scan, changes in anodic current at the work electrode was recorded. The surface morphology of the porous material was examined using scanning electron microscopy.

The electrocatalytic activity of the porous Au–Ni in 20 wt.% sugar and 0.2 M H_2SO_4 was characterized by cyclic voltammetry (CV). First, we tested the electrochemical behavior of the gold–nickel electrode without nanopores in the sugar sulfuric acid solution. Subsequently, the electrocatalytic behavior of the porous Au–Ni in the same sugar solution was investigated. During electrocatalytic property tests, the same three-electrode cell as shown in Fig. 1(b) was used. The Au–Ni and the porous Au–Ni electrodes were used as the work electrodes. The concentration of KCl filled in the reference electrode was kept at 3.0 M. The CV scanning range was controlled over a wide potential range of 0.0–1.0 V. The initial potential was 0.0 V. The polarity was set as positive. The scan rate was kept at 0.01 V/s. The data acquisition interval was set as 0.001 V. The quiet time was 2 s, and the sensitivity was 10^{-4} (A/V).

3. Results and discussion

Fig. 2(a) shows the global view of the porous structure of the Au–Ni material dealloyed in the diluted HNO_3. At higher magnification, gold-rich ligaments can be seen in Fig. 2(b). The width of the ligaments is in the range from 200 nm to 1 μm. In order to examine whether the porous structure is through the thickness or not, the electrochemically dealloyed Au–Ni wire was cut into two segments so that the cross-section was exposed as schematically shown in Fig. 3(a). Then, scanning electron microscopic observation was performed both on the surface and along the thickness direction. A typical area as highlighted in Fig. 3(a) was chosen to take SEM images. Such a image is shown in Fig. 3(b). Obviously, the dealloyed surface is porous as can be seen from the upper part of the SEM micrograph of Fig. 3(b). However, the cross-section area has the solid structure as shown in the lower left part of the SEM micrograph of Fig. 3(b). This indicates that the dealloying is not through the thickness.

The energy dispersive X-ray spectrum (EDS) of the porous gold alloy as shown in Fig. 4(a) was obtained, and the results are given in Fig. 4(b). From the peaks shown in Fig. 4(b), it can be seen that the major composition is Au. This will be further confirmed by the quantitative analysis. Ni peak also presents in the figure. There are several impurity elements such as C and Al. C could come from the conductive tape used for fixing the specimen on the SEM sample holder. Al signal is believed from the surface of the sample holder which is made of aluminum. The energy dispersive X-ray spectrum taken from the ligament area of site "A" in Fig. 2(b) reveals the same peaks of Au, Ni, C and Al elements.

The energy dispersive X-ray spectrum (EDS) quantitative results are shown in Fig. 5(a) and (b). It must be pointed out that the results shown in Fig. 5(a) were obtained form the EDS analysis of site "A" as marked in Fig. 2(b). This is a typical location showing the ligament structure. The ligaments are separated by pores. The results shown in Fig. 5(b) were obtained form the EDS analysis of site "B" as marked in Fig. 3(a). Site "B" is a typical location showing the pore structure. The EDS analysis of this site will give the information about the composition of materials within the pores.

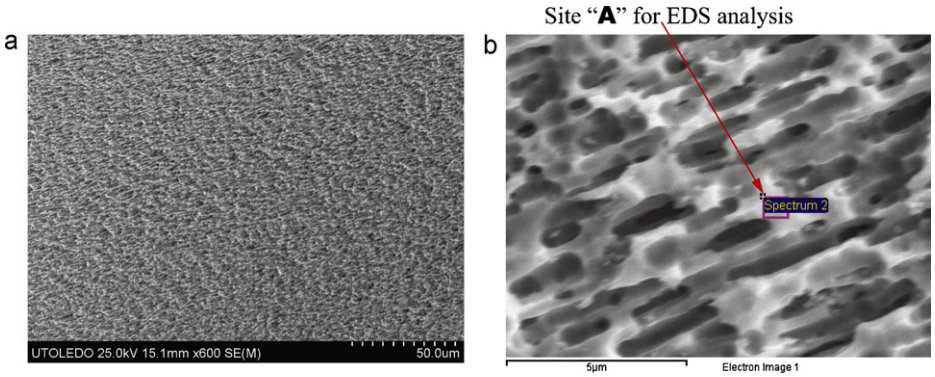

Fig. 2. Porous Au–Ni alloy prepared from electrochemical dealloying in 8.75% nitric acid: (a) low magnification SEM micrograph showing the global view of the porous structure and (b) highlighted gold-rich ligament.

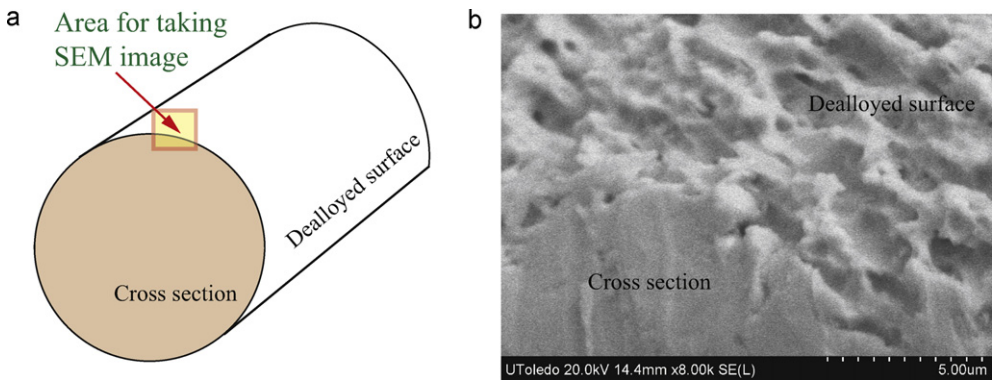

Fig. 3. Illustration of the Au–Ni alloy wire and the SEM image showing the cross-section and the dealloyed surface: (a) schematic of the Au–Ni alloy wire and (b) SEM image showing the cross-section and the dealloyed surface of the Au–Ni wire.

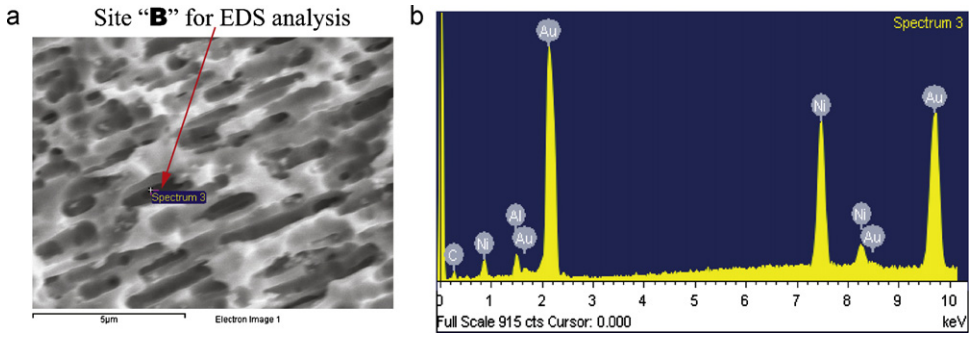

Fig. 4. SEM micrograph and EDS qualitative results: (a) SEM image showing the porous region and (b) EDS results of the pore region.

Comparing the results in Fig. 5(a) and (b), we can see that the material within the pore has different element contents than the ligament. The nickel content is much higher as shown in Fig. 5(b). This reveals the nonuniform in chemical composition of the porous structure. From the SEM analysis, it is obvious that gold-rich ligaments can successfully be prepared through the electrochemical dealloying and these ligaments show increased surface area. Nevertheless, the material within the pores are nickel-rich.

The formation of such a nonuniform porous Au–Ni material can be explained by the electrochemical dealloying mechanism as schematically shown in Fig. 6. In the initial stage of dealloying, a double layer was established at the interface of Au–Ni/HNO_3. Since the work electrode is an anode in the electrochemical reaction, NO_3^- attached to the Au–Ni metal and H^+ dispersed in the solution side as shown in Fig. 6(a). With positive potential in nitric acid, pitting occurred as shown in Fig. 6(b). Once a pitting cavity forms, the reactions inside the cavity are different from those at other locations. As shown in Fig. 6(c), Most of the Ni^{2+} generated from the tip of the ligaments can easily diffuse into the solution under the electric driving force due to the positive potential. Near the edge of the pit, Ni^{2+} is attracted by OH^- and reacts with OH^- to form an intermediate product, $Ni(OH)_2$. A portion of this intermediate product is eventually converted into $Ni(NO_3)_2$ due to the relatively high concentration of NO_3^- in the solution. It is noted that due to the positive potential at the Au–Ni work electrode, OH^- and NO_3^- are always attracted by the electrode and diffuse deep into the pit-

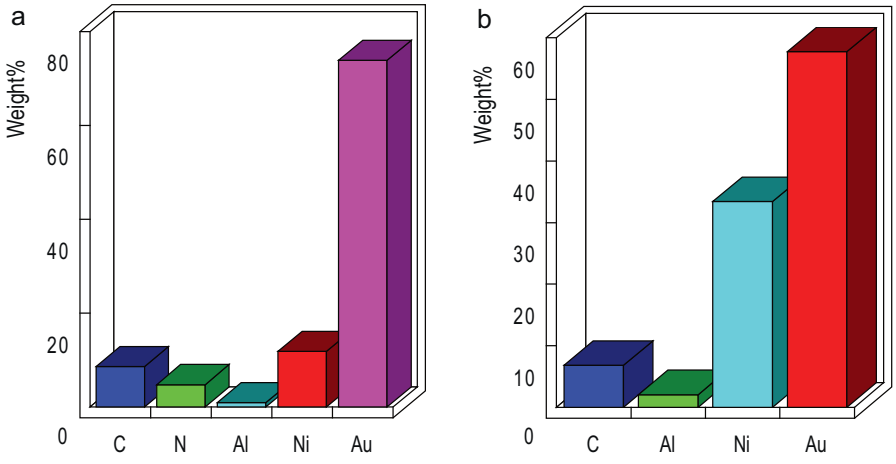

Fig. 5. EDS quantitative results: (a) composition of the ligament showing gold rich after dealloying and (b) composition of the pore region showing the increase of nickel content.

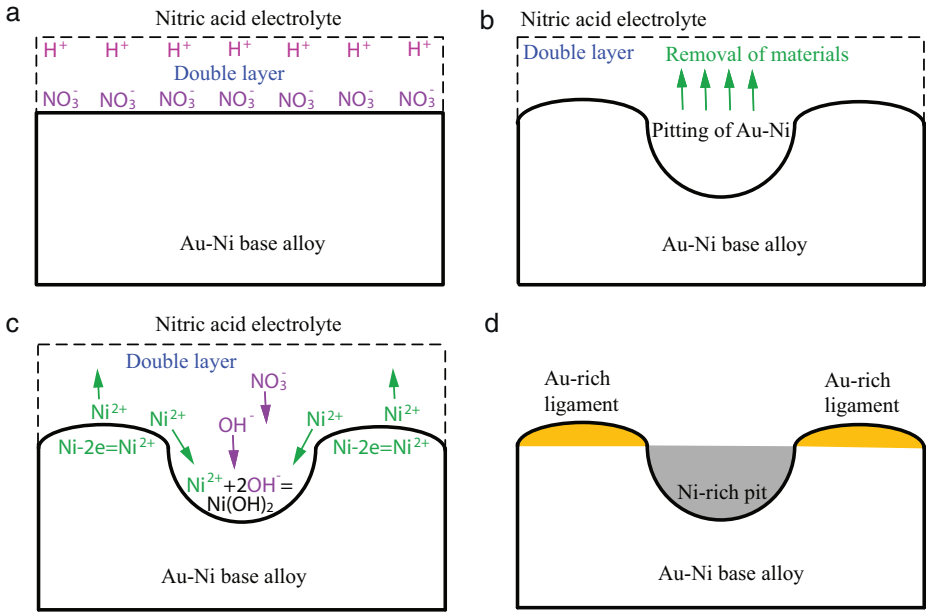

Fig. 6. Schematics showing the electrochemical dealloying mechanism: (a) double layer at the metal/electrolyte interface, (b) pitting of Au–Ni, (c) removal of Ni from the extruded regions, and (d) the Au-rich ligaments and the Ni-rich pit.

ting cavity. The dealloying of the Au–Ni alloy can be expressed by the following equation

$$Ni + 2H^+ + 2NO_3{}^- \rightleftharpoons H_2 \uparrow + Ni(NO_3)_2. \quad (1)$$

The main reaction at the cathode is hydrogen formation, i.e.

$$2H^+ + 2e^- \rightleftharpoons H_2 \uparrow . \quad (2)$$

At the anode, the selective dissolution of Ni consists of several electrochemical and chemical reactions as follows

$$Ni - 2e^- \rightleftharpoons Ni^{2+}, \quad (3a)$$

$$Ni^{2+} + OH^- \rightleftharpoons Ni(OH)^+, \quad (3b)$$

$$Ni(OH)^+ + OH^- \rightleftharpoons Ni(OH)_2, \quad (3c)$$

$$Ni(OH)^+ + NO_3^- \rightleftharpoons Ni(OH)(NO_3), \quad (3d)$$

$$Ni(OH)_2 + 2NO_3^- \rightleftharpoons Ni(NO_3)_2 + H_2O. \quad (3e)$$

The formation of the intermediate products such as $Ni(OH)_2$ and $Ni(OH)(NO_3)$ slow down the dissolution of Ni in the pit due to the spatial hindrance of these products. They slow down the mass transfer process in the pit and dealloying continues mainly in the ligament region. In addition to the spatial hindrance, another factor also causes the dissolution of nickel inside the pit to slow down. That factor is the change in the equilibrium for some of the above reactions. For example, the migration of the Ni^{2+} from the ligament surface into the pore will favor the righthand side reactions of both $Ni^{2+} + OH^- \rightleftharpoons Ni(OH)^+$ and $Ni(OH)^+ + OH^- \rightleftharpoons Ni(OH)_2$. The replenishment of Ni^{2+} will mainly from the dissolution of Ni in the ligament region, while the nickel in the pore region is passivated. Therefore, gold-rich ligaments and nickel-rich cavities are the main features as schematically shown in Fig. 6(d).

In order to examine the effect of nanopore on the electrocatalytic behaviors of electrodes in biodegradable fluids, comparative studies on the porous Au–Ni materials and the base Au–Ni alloy were conducted. The electrolyte consists of 20 wt.% of table sugar and 0.2 M sulfuric acid. The cyclic voltammograms are shown in Fig. 7(a) and (b). Fig. 7(a) is the cyclic voltammogram showing the change of current density at the Au–Ni alloy electrode in the 20 wt.% sugar

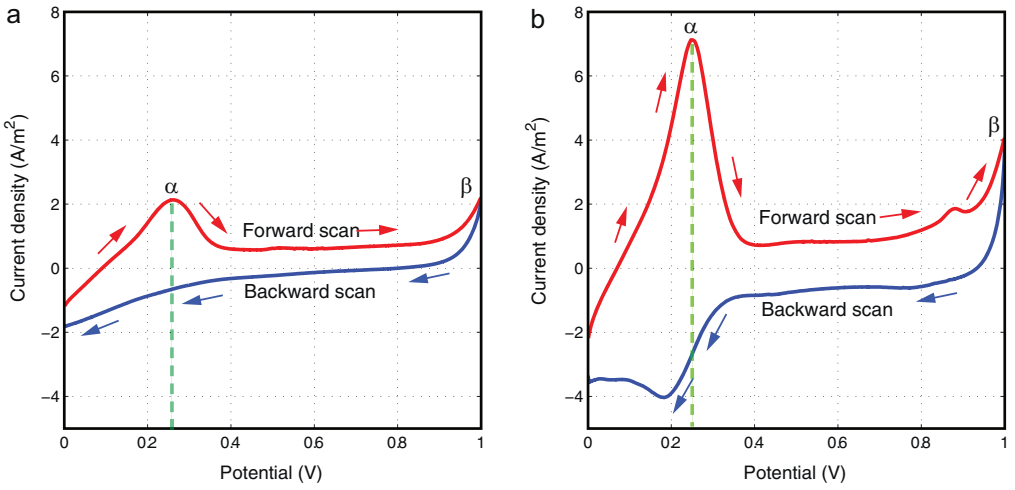

Fig. 7. Cyclic voltammograms showing electrochemical oxidation of carbohydrate on Au–Ni: (a) without nanopores and (b) with nanopores.

and 0.2 M H_2SO_4. It can be seen that there are two peaks related to oxidation reactions. The oxidation of sugar begins at the peak potential of 0.25 V as indicated by "Peak α" in Fig. 7(a). "Peak β", corresponding to the potential larger than 0.975 represents the oxygen generation reaction. Fig. 7(b) shows the cyclic voltammogram of the porous Au–Ni. The current density at the porous electrode, as shown in Fig. 7(b), was calculated based on the initial area of the alloy before dealloying. Both α and β peaks are higher than those shown in Fig. 7(a) for the case of bulk electrode. It is also found that the cyclic voltammogram of the bulk Au–Ni as shown in Fig. 7(a) has the reaction-controlled feature followed by mass transfer controlled mechanism. The same behavior was observed for the porous Au–Ni electrode. However, the current density of the porous Au–Ni is as four times high as that of the bulk nickel electrode. The results reveal that the porous electrode is more effective than the bulk Au–Ni in electrochemical catalytic oxidation of the carbohydrate solution.

4. Conclusions

Porous gold–nickel alloy has successfully been prepared by electrochemical dealloying in 8.75 wt.% nitric acid. The surface morphology of the dealloyed material consists of gold-rich ligaments and nickel-rich pores. The reason for the formation of nonuniform structure is due to the intermediate product formation. Nickel hydroxide in the pore slows down the further dissolution of nickel. Comparative studies on the porous Au–Ni and the bulk Au–Ni alloy show that the porous electrode is more effective than the bulk electrode in electrochemical catalytic oxidation of biodegradable fluids. The cyclic voltammograms of the bulk Au–Ni and porous Au–Ni show the same electrochemical oxidation mechanism, i.e. both reaction and mass transfer controlled feature. However, the current density at the porous Au–Ni is as four times high as that at the bulk nickel electrode.

Acknowledgments

This work is supported by the research start-up fund and Summer Faculty Research Fellowship from The University of Toledo. We appreciate Mr. Abraham Avalos for his help in electron microscopic analysis.

References

[1] A. Lunnan, Energy Policy 25 (1997) 573.
[2] J. Dobereiner, J.S.A. Neto, D.B. Arkcoll, Stud. Environ. Sci. 16 (1982) 431.
[3] J.X. He, S. Baharani, Y.X. Gan, Res. Lett. Nanotechnol. (2009) 313962.
[4] W.C. Li, T.J. Balk, Materials 2 (2009) 2496.
[5] F. Jia, C. Yu, L. Zhang, Electrochem. Commun. 11 (2009) 1944.
[6] Y.X. Gan, Adv. Mater. Syst. Energy Conv. Nova. Sci. Pub. N. Y. (2010) 117.
[7] H. Hakamada, M. Mabuchi, Scripta Mater. 56 (2007) 1003.
[8] G.B. Smith, A.I. Maaroof, A. Gentle, Opt. Commun. 271 (2007) 263.
[9] H. Zhou, N. Jin, W. Xu, Chin. Chem. Lett. 18 (2007) 365.
[10] T. Tesfamichael, N. Motta, T. Bostrom, J.M. Bell, Appl. Surf. Sci. 253 (2007) 4853.
[11] Y. Ding, M. Chen, J. Erlebacher, J. Am. Chem. Soc. 126 (2004) 6876.
[12] S.O. Kucheyev, J.R. Hayes, J. Biener, T. Huser, C.E. Talley, A.V. Hamza, Appl. Phys. Lett. 89 (2006) 053102.
[13] D. Kramer, R.N. Viswanath, J. Weissmüller, Nano Lett. 4 (2004) 793.
[14] J. Rösler, O. Näth, S. Jäger, F. Schmitz, D. Mukherji, Acta Mater. 53 (2005) 1397.
[15] C. Basheer, S. Swaminathan, H.K. Lee, S. Valiyaveettil, Chem. Commun. 3 (2005) 409.
[16] R. Zeis, A. Mathur, G. Fritz, J. Lee, J. Erlebacher, J. Power Sources 165 (2007) 65.
[17] D.A. Crowson, D. Farkas, S.G. Corcoran, Scripta Mater. 56 (2007) 919.
[18] D. Lee, X. Wei, X. Chen, M. Zhao, S.C. Jun, J. Hone, E.G. Herbert, W.C. Oliver, J.W. Kysar, Scripta Mater. 56 (2007) 437.